PASSIVE SEISMIC SOURCE LOCALIZATION VIA CRS ATTRIBUTES

B. Schwarz, A. Bauer, and D. Gajewski

email: *benjamin.schwarz@uni-hamburg.de*

keywords: *stacking, passive seismics, moveout, NIP tomography*

ABSTRACT

The common-reflection-surface (CRS) stack can be viewed as a physically justified extension of the classical CMP stack, utilizing redundant information not only in a single but in several neighboring CMP gathers. The zero-offset CRS moveout is parameterized in terms of kinematic attributes, which utilize reciprocity and raypath symmetries to describe the two-way process of the actual wave propagation in active seismic experiments by the propagation of auxiliary one-way wavefronts. For the diffraction case, only the attributes of a single one-way wavefront, originating from the diffractor are sufficient to explain the traveltime differences observed at the surface. While paraxial ray theory gives rise to a second-order approximation of the CRS traveltime, many higher-order approximations were subsequently introduced either by squaring the second-order expression or by employing principles of optics and geometry. It was recently discovered that all of these higher-order operators can be formulated either for the optical projection or in an auxiliary medium of a constant effective velocity. Utilizing this duality and the one-way nature of the CRS parameters, we present a simple data-driven stacking scheme that allows for the inversion of the a priori unknown excitation time of a passive seismic source. In addition, we demonstrate with a simple data example that the output of the suggested workflow can directly be used for subsequent focusing-based NIP tomography, leading to a reliable localization in depth.

INTRODUCTION

Stacking still can be considered one of the most reliable processes in seismology and its origins date back to the late 60s (Mayne, 1962). In both, active and passive regimes, the coherent summation of amplitudes can lead to a significant increase of the signal-to-noise ratio and especially weak events, which were barely recognizable in the raw data can be made accessible for further processing and interpretation (Shearer, 1990). With the introduction of normalized velocity spectra (Taner and Koehler, 1969), the process of stacking can in principle be fully automized. The common-reflection-surface (CRS) stack is an extension of the classical common-midpoint (CMP) stack, in which many neighboring midpoints are jointly described by a traveltime surface (Jäger et al., 2001). While a decrease in the noise level is a virtue on its own, the estimated CRS operators can also be used for efficient prestack data enhancement, like trace interpolation or regularization (Baykulov and Gajewski, 2009). In addition, the CRS traveltime moveout expression is parameterized in terms of kinematic attributes of fictitious one-way propagation experiments (Hubral, 1983), which can be utilized for various applications, ranging from multiple suppression (Dümmong and Gajewski, 2008), diffraction separation (Dell and Gajewski, 2011), geometrical spreading compensation (Hubral, 1983), Fresnel zone estimation for migration (Hubral et al., 1993) to advanced depth velocity model building via NIP tomography (Duveneck, 2004).

Although originally, a second-order expressions followed from the propagator formalism by Bortfeld (1989) in paraxial ray theory, a hyperbolic operator is commonly favored, since it proved to provide higher

accuracy in the presence of predominantly vertical heterogeneity (Schleicher et al., 1993). Alongside the co-existing multifocusing approach, several higher-order CRS formulations have been introduced in recent years (Landa et al., 2010; Fomel and Kazinnik, 2013; Schwarz et al., 2014b). By extending the work of de Bazelaire (1988) and Höcht et al. (1999), Schwarz et al. (2014a, 2015) demonstrated that all these higher-order expressions, including the commonly used hyperbolic CRS operator, can either be formulated for the optical projection or an effective analog of the true kinematics of the wave propagation. In these different domains, heterogeneity is accounted for either by a shift in time or in velocity. In addition, they provided an alternative CRS parameterization, in which dip, curvature and heterogeneity effects are handled by separate attributes. In that frame, they introduced a CRS-type extension of de Bazelaire's osculating equation, which allows for a free transformation between the optical and the effective domain.

While in active seismic acquisitions, the location and the excitation time of the source is generally known, the processing is primarily concerned with resolving and inverting the structure and properties of the traversed medium (Sheriff and Geldart, 1995). A passive seismic problem, in contrast, faces the additional difficulties of unknown source characteristics. Closing the gap between traditional large-scale earthquake seismology and controlled-source seismic exploration, Rutledge and Phillips (2003) found that microseismicity can be utilized to image the process of the stimulation of hydraulic fracturing. Besides its essential use in the imaging of low-amplitude phases like precursors on continental or even global scales (Shearer, 1990), stacking proved to be also a useful tool for the localization and characterization of microseismic events (Gajewski et al., 2007; Zhebel et al., 2011). Following from symmetry principles, the CRS attributes describe actual two-way propagation by an auxiliary one-way kinematic point source experiment. In this work, we introduce a passive seismic stacking operator, that is formulated in terms of the CRS attributes. By utilizing the aforementioned duality of higher-order moveouts, we suggest a simple strategy to extract the a priori unknown excitation time of a passive seismic event and propose the subsequent use of NIP tomography (Duveneck, 2004) to jointly invert for the depth location and the overburden velocity model.

THEORY

CRS stack and attributes

The common-reflection-surface (CRS) stack (Jäger et al., 2001) can be viewed as a generalization of the classical CMP stack method (Mayne, 1962), in which the coherent summation follows a moveout surface, which extends over several neighboring CMP gathers. Consequently, in the 2D case, the zero-offset CRS stacking operator depends on three parameters, which have to be estimated via coherence analysis. Despite its higher dimensionality, the CRS moveout is expressed in terms of surface-related kinematic wavefield attributes, which exploit raypath symmetries to describe the general two-way reflection kinematics by two fictitious one-way experiments (Hubral, 1983). While the moveout in the common-reflection-point (CRP) gather (see Figure 1), can be fully described by the attributes of the normal-incidence-point (NIP) wave thought to originate at the reflection point of the zero-offset ray, traveltime differences in the zero-offset section are governed by an exploding reflector experiment around the NIP, the so-called normal (N) wave experiment (Hubral, 1983). In midpoint (x_m) and half-offset (h) coordinates the hyperbolic CRS operator (Schleicher et al., 1993; Jäger et al., 2001) takes the form

$$t = \sqrt{\left(t_0 + \frac{2\sin\alpha_0}{v_0}\Delta x_m\right)^2 + \frac{2t_0\cos^2\alpha_0}{v_0}\left(\frac{\Delta x_m^2}{R_{\text{N}}} + \frac{h^2}{R_{\text{NIP}}}\right)} \quad , \tag{1}$$

where t_0 is the zero-offset two-way reference time, α_0 denotes the emergence angle and R_{NIP} and R_{N} are the curvature radii of the NIP and the normal wave, measured at the central midpoint location x_0. The deviation from the central midpoint location is Δx_m. For the diffraction case, both conceptual wavefronts coincide. Thus, we arrive at the CRS diffraction operator by setting $R_{\text{N}} = R_{\text{NIP}}$. In the symmetric zero-offset configuration, it reads

$$t = \sqrt{\left(t_0 + \frac{2\sin\alpha_0}{v_0}\Delta x_m\right)^2 + \frac{2t_0\cos^2\alpha_0}{v_0 R_{\text{NIP}}}\Delta x_m^2} \quad . \tag{2}$$

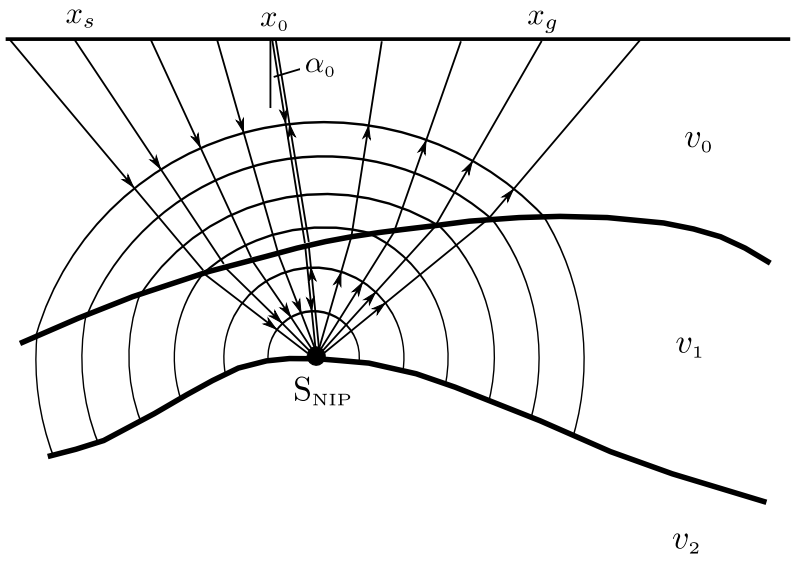

Figure 1: Based on the reciprocity of ray paths, the normal-incidence-point (NIP), or more generally, the common-reflection-point (CRP), can be viewed as a fictitious source in depth (Hubral, 1983). For Snell's law to be fulfilled only certain emission angles are realized and thus, for a general reflection, the source and receiver angles are coupled in the NIP or the CRP gather. For a diffraction, source and receiver contributions are decoupled and the NIP wave attributes α_0 and R_{NIP} are sufficient to describe the traveltime moveout observed at the surface.

Please note that despite the chosen notation, the traveltime difference $\Delta t = t - t_0$ is needed to perform the CRS stack. As follows from equation (1), the presented conventional CRS parameterization implies that the moveout Δt is a function of the reference traveltime t_0, which corresponds to the traveltime of the zero-offset reference ray. Following from reciprocity, Hubral (1983) concluded that in order to accurately describe the moveout of reflected events, the conceptual NIP wave, illustrated in Figure 1 must travel at half the medium velocity. For the actual true velocity distribution, accordingly, a seismic point source placed at the normal-incidence-point would take $t_0/2$ to arrive at the central midpoint location at the surface. In the next subsection, we will briefly review the duality of higher order CRS-type moveouts, which will prove to bear an interesting potential for passive seismic applications.

Dual description of higher-order moveouts

As mentioned before, the CRS moveout in its conventional parameterization depends on the zero-offset reference time t_0. Following the works of de Bazelaire (1988) and Höcht et al. (1999), Schwarz et al. (2014a, 2015) found that all higher-order CRS-type stacking operators, including multifocusing (Gelchinsky et al., 1999), can be formulated in terms of the CRS attributes in two different ways, one accounting for overburden heterogeneity by the application of a constant shift in velocity, the other, in correspondence with de Bazelaires shifted hyperbola, by a constant shift of the reference time. Since this duality is central for the formulation of the suggested CRS-based passive strategy, Figure 2 conceptually illustrates the complementary nature of the two mechanisms. As can be observed on the left side of Figure 2, in the conventional CMP stack, shown for the historically important case of horizontal layering, the actual layered velocity structure is replaced by a constant effective velocity, which forms the foundation of seismic velocity analysis (Taner and Koehler, 1969). For the shifted hyperbola by de Bazelaire (1988), in contrast to the conventional approach, the actual vertically heterogeneous medium is replaced by a constant shift of the reference time, which in the simple ray picture on the right side of Figure 2 corresponds to the optical projection of the true NIP wave propagation observed at the registration surface (de Bazelaire, 1988). According to Höcht et al. (1999) and Schwarz et al. (2014b), both mechanisms can be related to the CRS

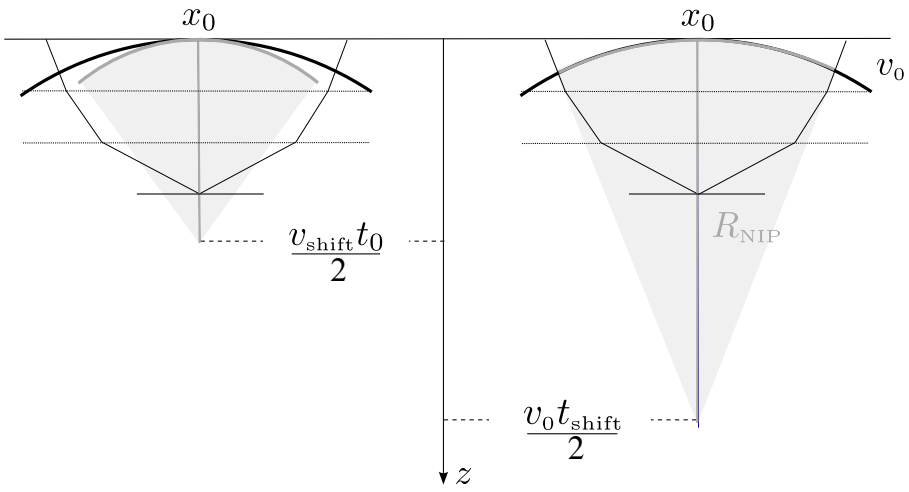

Figure 2: Illustration of the relationship between wavefront curvature and reference traveltime in the classical CMP stack. In case of a single planar target reflector with constant velocity overburden, the radius of wavefront curvature and the distance to the reflector coincide and the hyperbolic approximation is exact, while they differ for the heterogeneous case. The solid black lines represent the actual raypath, whereas gray colors indicate the velocity shift and time shift mechanism, respectively. Please note that the case of vertical heterogeneity is chosen for illustration purposes, but that the concept also applies to more general laterally inhomogeneous media.

attributes via the expressions

$$v_{\text{shift}} = \frac{v_{\text{NMO}}}{\sqrt{1 + (v_{\text{NMO}}/v_0)^2 \sin^2 \alpha_0}} \quad , \tag{3a}$$

$$t_{\text{shift}} = \frac{2R_{\text{NIP}}}{v_0} \quad , \tag{3b}$$

with the NMO velocity

$$v_{\text{NMO}} = \sqrt{\frac{2v_0 R_{\text{NIP}}}{t_0 \cos^2 \alpha_0}} \quad . \tag{4}$$

Please note that despite the simplified illustration in Figure 2, expressions 3 are even valid for the more general case of lateral heterogeneity. Following from the implicit CRS parameterization, Schwarz et al. (2015) found that velocity shifts can be transformed into time shifts and vice versa via the generalized osculating equation

$$p_{\text{shift}}^2 = p_{0x}^2 + \frac{t_0}{t_{\text{shift}}}(p_0^2 - p_{0x}^2) \quad , \tag{5}$$

where, for convenience, $p_{\text{shift}} = 1/v_{\text{shift}}$ and $p_0 = 1/v_0$ denote the effective slowness and the slowness near the surface. The ray parameter near the surface p_{0x} is directly related to the event dip in the zero-offset section. According to this equation, it can be shown that all CRS-type operators of higher order than two can be transformed to the optical domain or the effective medium by re-parameterizing the operator in terms of 3 and by applying the osculating condition (5). In the following, we use the zero-offset CRS diffraction response (2) to introduce a passive seismic stacking operator, which is parameterized in terms of the kinematic attributes of the NIP wave.

From active to passive seismics

As emphasized before, the fictitious concept of the NIP wave, utilizing raypath symmetries and reciprocity, proved to be very useful in reducing the complex two-way ray geometry of a reflection experiment to

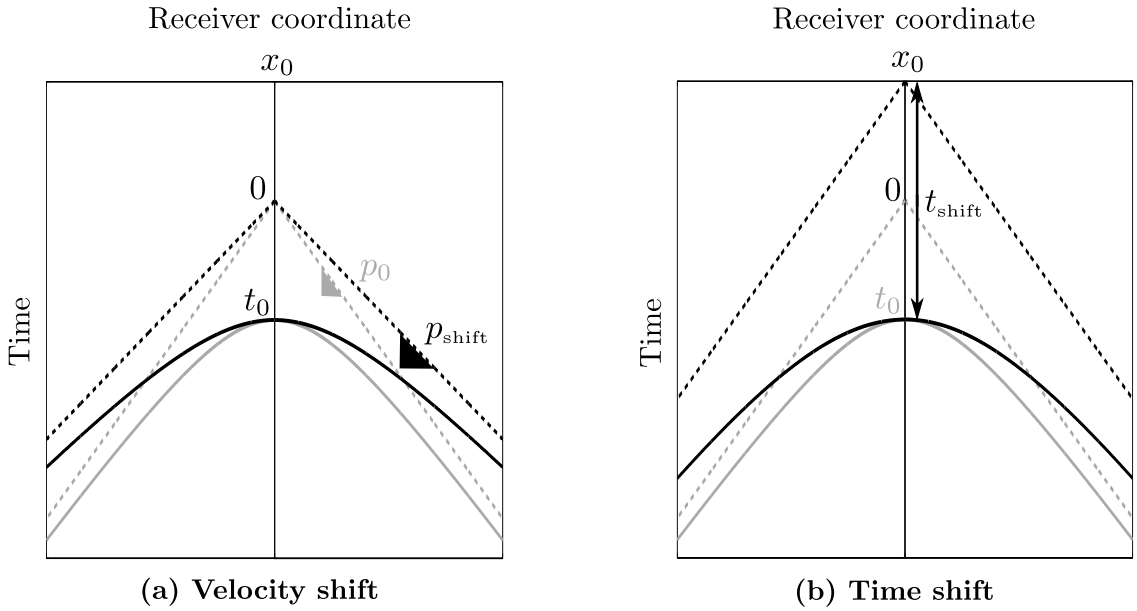

Figure 3: Two different ways to change the suggested passive seismic moveout expression to account for heterogeneity: (a) Classical velocity spectra approach, where the velocity is perturbed (Taner and Koehler, 1969). (b) Application of a time shift t_{shift} (de Bazelaire, 1988). Actual traveltime curves are in bold lines, their respective asymptotes are dotted. Both shifts lead to a comparable perturbation of moveout (indicated in bold black). While the time-shifted moveout is independent of the true reference time, the effective medium counterpart incorporates t_0 and therefore can be used for the inversion of the passive source excitation time.

the much simpler geometry of a one-way propagating wavefront, which leads to the same description of the moveout (Hubral, 1983). For a passive experiment, this one-way experiment is physically real and the fictitious source can in this case be identified with the true source of the passive event. Due to the coincidence of the up and down-going ray paths in the zero-offset section, the moveout of a one-way propagating wave follows from halving the active source CRS diffraction operator (2),

$$\Delta t = \sqrt{\left(t_0 + \frac{\sin\alpha_0}{v_0}\Delta x_g\right)^2 + \frac{t_0 \cos^2\alpha_0}{v_0 R_{\text{NIP}}}\Delta x_g^2} - t_0 \quad , \tag{6}$$

in which the midpoint displacement Δx_m is replaced by the relative lateral receiver distance Δx_g. Formally, as stressed before, this expression is exactly equivalent to the diffraction case in the zero-offset configuration, with the only difference that for the active experiment the NIP wave, per definition, travels at half the actual medium velocity, wehereas in the considered passive scenario, the propagation takes place at the actual velocity. By re-parameterization according to equation (5), which is equally valid for the passive seismic case, this operator can either be formulated with a time shift or a velocity shift mechanism to account for overburden heterogeneity. The passive traveltime can thus be generalized as

$$\begin{aligned} t &= t_s + t_0 + \Delta\hat{t}(\hat{t}_0, \hat{p}) \\ &= t_s + t_0 + \sqrt{(\hat{t}_0 + p_{0x}\Delta x_g)^2 + (\hat{p}^2 - p_{0x}^2)\Delta x_g^2} - \hat{t}_0 \quad , \end{aligned} \tag{7}$$

where $(\hat{t}_0, \hat{p})$ corresponds either to the time-shifted one-way reference time $t_{\text{shift}} = R_{\text{NIP}}/v_0$ and the near-surface slowness p_0 or the effective medium counterparts t_0 and p_{shift} (Schwarz et al., 2015). The time shift and the velocity shift approach are compared in a conceptual sketch shown in Figure 3. While the moveouts, due to the aforementioned symmetries, are very similar for the active zero-offset case and a passive setting, the main difference constitutes in the fact that the excitation time of the passive source,

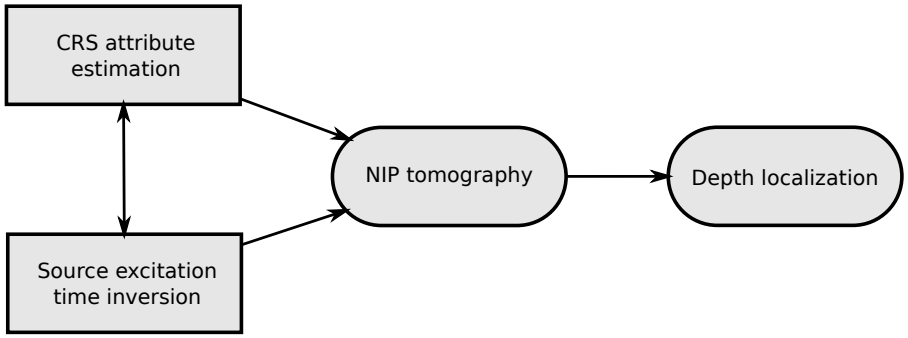

Figure 4: Overview of the suggested passive seismic workflow. In the first stage, the horizontal slopes and time shifts, which can be translated into the CRS parameters α_0 and R_{NIP}, are estimated using the time-shifted version of the passive operator. Subsequently, the effective medium moveout is applied to gain the source excitation time t_s of the respective passive event. After correcting for the source time, the CRS attributes are fed into NIP tomography resulting in a kinematically inverted velocity model and the source locations in depth.

denoted by t_s is generally not known for the latter case. In the following, we suggest a hybrid scheme, in which subsets of the generalized operator (7) are used to sequentially measure the attributes p_{0x}, t_{shift} and t_0, the latter allowing a direct moveout-based inversion of the source time t_s.

WORKFLOW AND DATA EXAMPLE

Following the introduction of the passive seismic strategy, we will demonstrate the principal applicability of the suggested scheme to a passive seismic dataset. From a kinematic viewpoint, a passive seismic experiment is characterized by the additional complication of the unknown source time. Thus, we simulate a passive seismic experiment by modeling the response of three buried seismic sources in a vertically and laterally heterogeneous background and subsequently shift the recorded events by an arbitrary amount in time. The chosen simulated excitation times of the three sources, as well as their true locations and the velocity structure in depth are displayed in Figure 5. Figure 6 shows the modeled data with a trace spacing of 25 m and a dominant event frequency of 30 Hz (chosen for convenience) without time delays applied (left) and the simulated passive acquisition with time-shifts applied (right). In addition, we chose to add a reasonable amount of random noise to the data, to ensure a more realistic setting. The chosen receiver apertures vary from 300 m, for the initial dip search, to 1000 m and 2000 m for the curvature-related measurements of the shifted reference and the source time. While, for convenience, the initial one-parameter searches constitute in fine-meshed grid searches, parameters are subsequently refined using a Nelder Mead simplex optimization algorithm (Nelder and Mead, 1965). As illustrated in Figure 4, the initial CRS parameter estimation is followed by an automated correction for the estimated source times, whose results are then fed into the NIP tomographic inversion scheme by Duveneck (2004).

Attribute estimation

In the following, we suggest a simple and stable scheme to sequentially measure and refine all unknowns in equation (7) via redundancy-exploiting multi-parameter coherence analysis. The measure of coherence, in accordance with current implementations of the CRS stack and similar to conventional velocity analysis is the normalized semblance coefficient (Taner and Koehler, 1969). The first step of this strategy is equivalent to the plane wave search suggested for the pragmatic CRS approach (Jäger et al., 2001) and makes use of the first-order subset of the generalized passive operator (7)

$$\Delta t \approx \Delta t(p_{0x}) = p_{0x}\Delta x_g \quad . \tag{8}$$

Since the slope attribute p_{0x}, i.e. the local traveltime dip, is independent of the choice of the auxiliary medium, i.e. the optical projection space and the effective medium, the actual reference traveltime and the

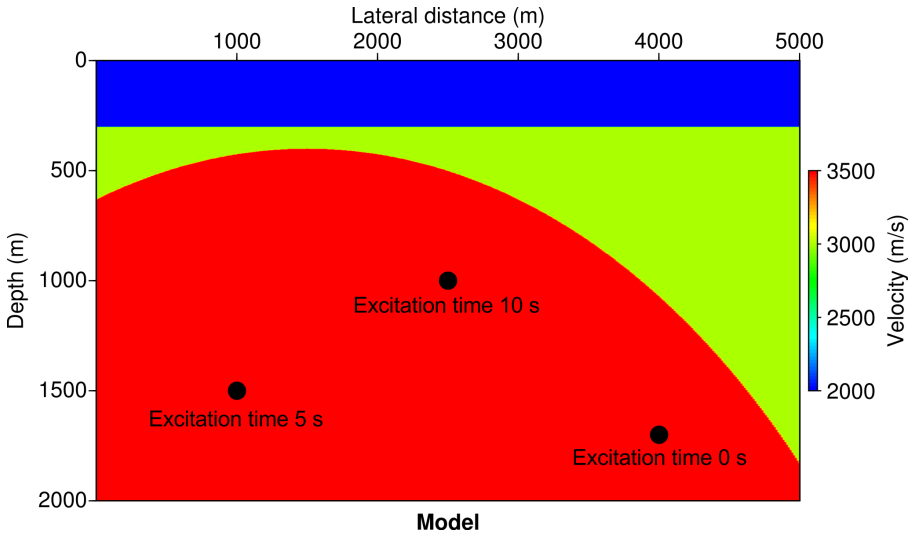

Figure 5: 2D velocity model used for the modeling of the considered passive seismic events. While the upper part is laterally homogeneous, the second interface reveals a finite curvature which results in lateral velocity variations in the deeper part. The locations of the passive seismic sources are represented by circles and their respective simulated excitation times are annotated.

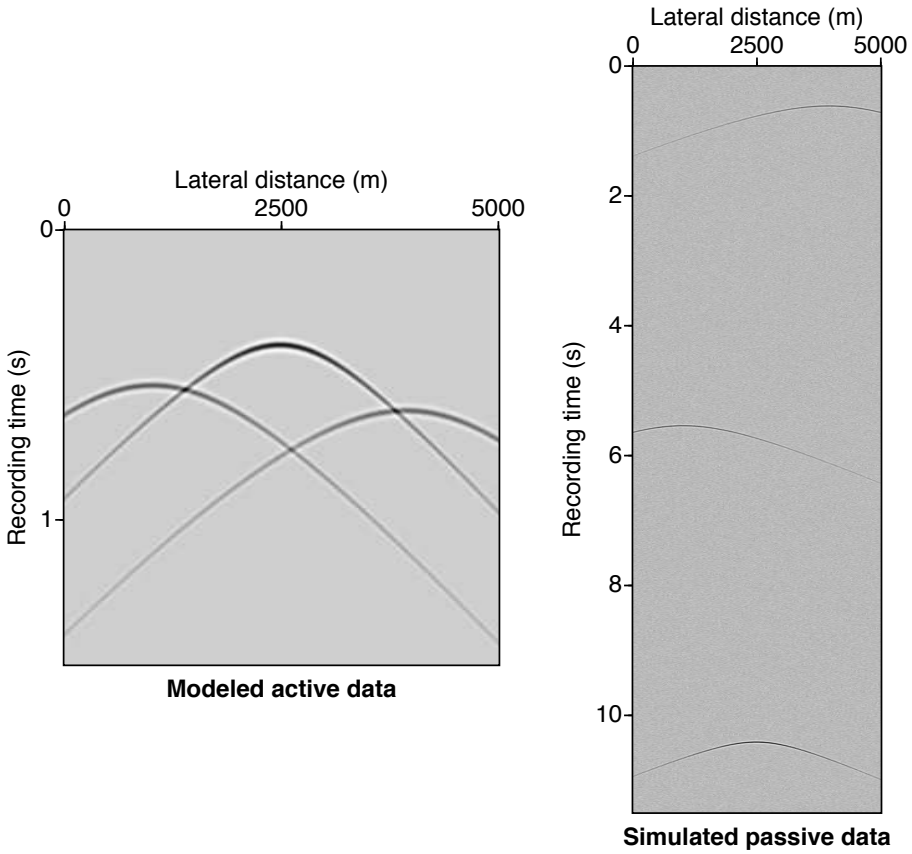

Figure 6: Synthetic passive seismic data, generated via ray modeling for the velocity distribution shown in Figure 5. To simulate a passive seismic experiment, the raw modeled events (left) were shifted in time by either 0, 5 or 10 s (compare Figure 5) and a reasonable amount of noise was added (right).

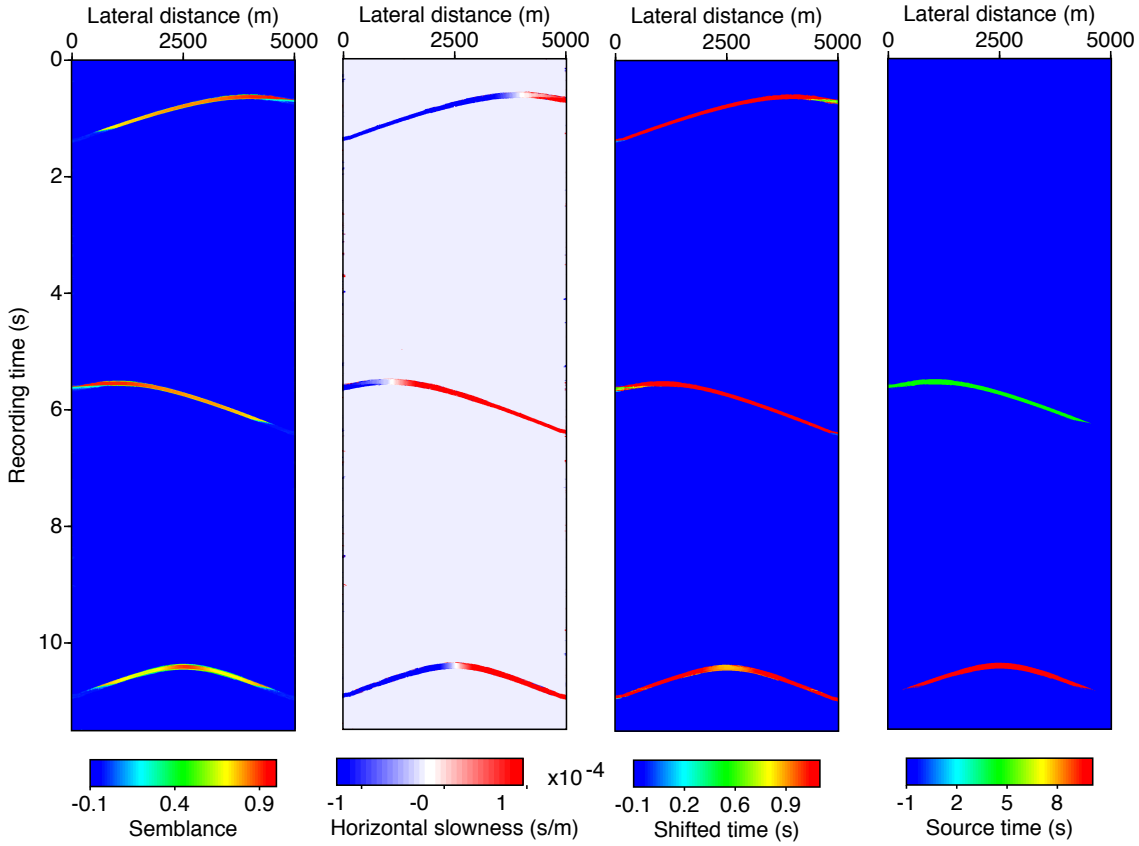

Figure 7: Attribute estimation results for the considered synthetic passive experiment. All attributes were estimated in a data-driven fashion and the coherence of the subsequent estimation step of the proposed strategy was used for thresholding, resulting in reasonably efficient application. While the left three panels are also available in active seismic applications, the estimation results of the source time displayed on the right is a new ingredient in the passive seismic workflow and crucial for the subsequent localization in depth.

source excitation time both do not need to be known for this first measurement. The second step of the suggested pragmatic approach consists of a second-order moveout measurement for the optical projection of the problem, i.e. the time-shift mechanism. According to Schwarz et al. (2014a), time-shifted moveouts in general as well do not depend on the actual reference time and therefore can also be accurately measured without the knowledge of t_0 and t_s

$$\Delta t = \Delta t(p_{0x}, t_{\text{shift}}) = \sqrt{(t_{\text{shift}} + p_{0x}\Delta x_g)^2 + (p_0^2 - p_{0x}^2)\Delta x_g^2} - t_{\text{shift}} \quad , \tag{9}$$

where $p_0 = 1/v_0$ is the inverse of the near-surface velocity, i.e. the near-surface slowness at the receiver. Since the horizontal slowness was gained in the preceding dip measurement (8), this second step, based on equation (9), consists again of a one parameter search, in this case for the shifted reference time t_{shift}.

While until now, only the time-shift mechanism was utilized, the third and final step of the suggested pragmatic scheme makes use of the second face, i.e. the velocity-shifted version of the passive moveout operator (7). In the considered frame of a passive seismic experiment, this dependency of the velocity-shifted moveout on the actual reference time t_0 proves to be very valuable and allows for the inversion of the source excitation time. We have, again based on the preceding measurements of p_{0x} and t_{shift}, a

one-parameter optimization problem

$$t = t_s + t_0 + \sqrt{(t_0 + p_{0x}\Delta x_g)^2 + [p^2_{\text{shift}}(t_0) - p^2_{0x}]\Delta x_g^2} - t_0$$
$$= t_s + \sqrt{(t_0 + p_{0x}\Delta x_g)^2 + [p^2_{\text{shift}}(t_0) - p^2_{0x}]\Delta x_g^2} \quad , \tag{10}$$

with p_{shift} defined via the generalized osculating equation, which, as mentioned before, is equally valid for active and passive seismic experiments.

Figure 7 shows the estimated attributes following the proposed strategy for the suggested synthetic example. While due to the added noise level, the passive events are hardly recognizable over the full considered receiver line, in the attributes sections the coherent energy is well recognizable. The consistently high coherence values along the events, shown in the left attribute panel, indicate the appropriate fit of the passive operator in the considered aperture range. Being a local measurement, the slope estimation, which is shown in the second panel of Figure 7, performed reasonably stable and resulted in the expected smooth behavior along the events. In addition, the large range of slope values indicates the good ray coverage of point-like passive seismic events, illuminating large portions of the underlying velocity model (compare Figure 5). Being related to the wavefront curvature measured at the surface, the shifted reference traveltime and the source excitation time need to be estimated in larger apertures. Nevertheless, the corresponding attribute panels shown on the right of Figure 7 reveal a generally smooth distribution of values along the events. Especially the source times are estimated with reasonable accuracy, showing a very good correspondence with the exact values of 0 s, 5 s, and 10 s. It can be concluded that for the considered synthetic example, the proposed strategy allows for a robust fully automatic estimation not only of the dip and curvature moveout contributions, but also for a reasonably accurate inversion of the unknown excitation times. As will be demonstrated in the following, every passive event has a characteristic source time and therefore allows for a data-driven correction of the individual events.

Depth localization via NIP tomography

Due to the formal equivalence of the fictitious NIP wave and the true passive experiment, The extracted attributes can directly be used for efficient localization and joint velocity inversion in depth. The conventional inversion needs the emergence angle, the NIP wave radius and the true propagation time of the reference ray as input. As a result, the locations of the individual normal-incidence-points and the traversed overburden velocity structure are inverted and can be jointly displayed for interpretational purposes. In the available implementation by Duveneck (2004) the picking of locally coherent contributions is performed fully automatically using the coherence and stacked sections. In order to be performed, NIP tomography requires, as mentioned before, the knowledge of the true propagation time of the respective reference rays. Thus, the estimated passive attributes $(p_{0x}, t_{\text{shift}})$ need to be transformed to $(\alpha_0, R_{\text{NIP}})$ and, in addition, all required input sections must be corrected for the individual estimated event source times. Since NIP tomography is commonly used on two-way reflection data, an additional factor of two has to be applied on the time axes.

Figure 8 shows the respective transformed and corrected sections for the considered synthetic dataset. As can be observed the source time estimation and correction was reasonably successful in reproducing the raw modeled data displayed on the right side of Figure 6. The near-surface velocity of v_0 =2000 m/s was used as the starting velocity model for NIP tomography. In Figure 9 the corresponding NIP localization results are superimposed on the velocity model. The individual NIP locations do not correspond with the actual source positions denoted by the three circles. Figure 10 shows the result of NIP tomographic inversion, where the NIP locations correspond to the locally estimated positions of the passive sources. Due to the joint inversion, NIP tomography is not only capable of providing a reasonable passive localization, but also leads to a kinematically sound inversion of the traversed velocity structure.

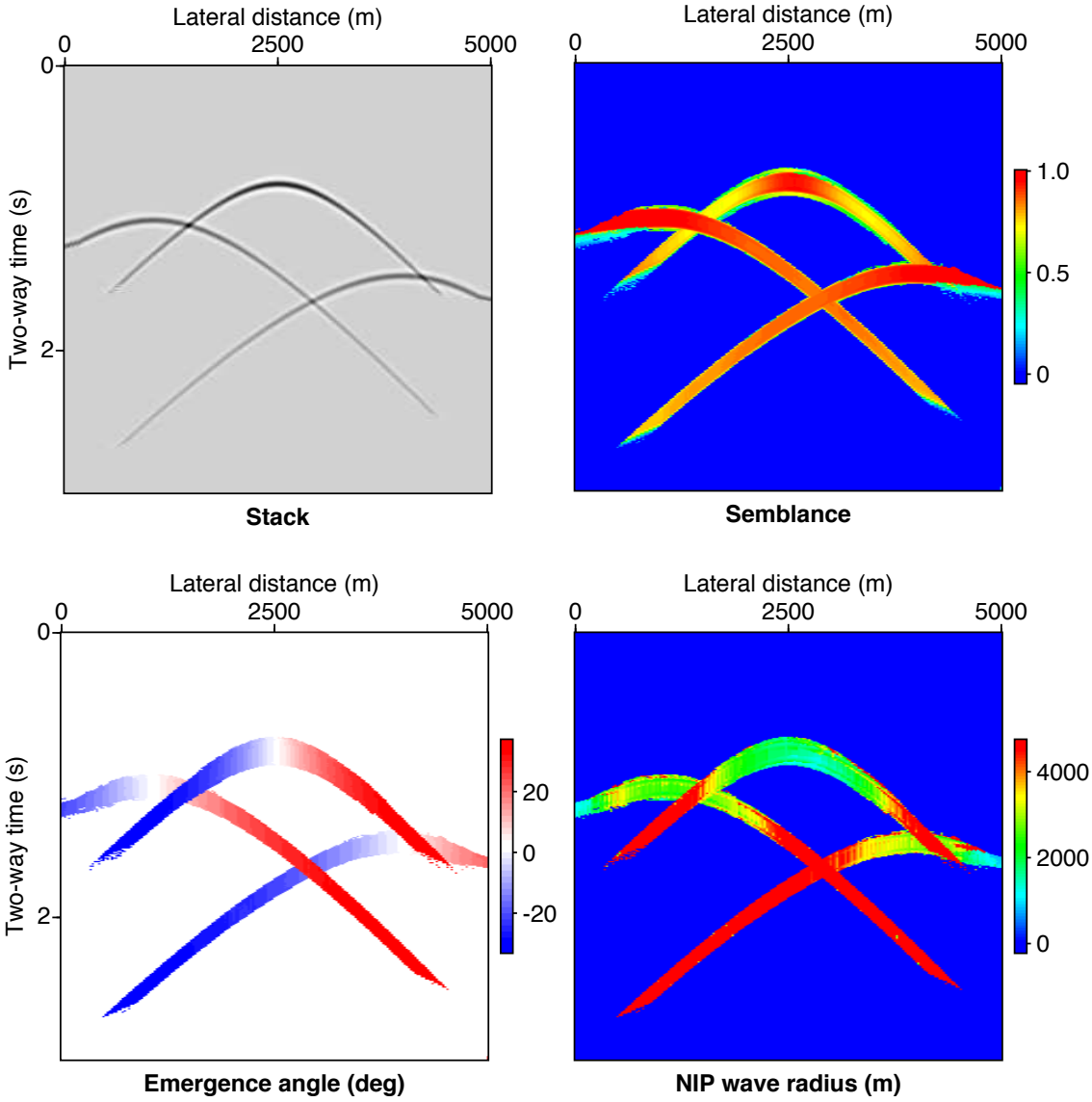

Figure 8: For NIP tomography to be performed, the estimated attributes $(p_{0x}, t_{\text{shift}})$, as well as the coherence and the stacked section need to be corrected for the individual source excitation times. Comparison of the corrected stacked section with the modeled data displayed in Figure 6 reveals that the event locations in time could be reproduced reasonable well by the suggested strategy.

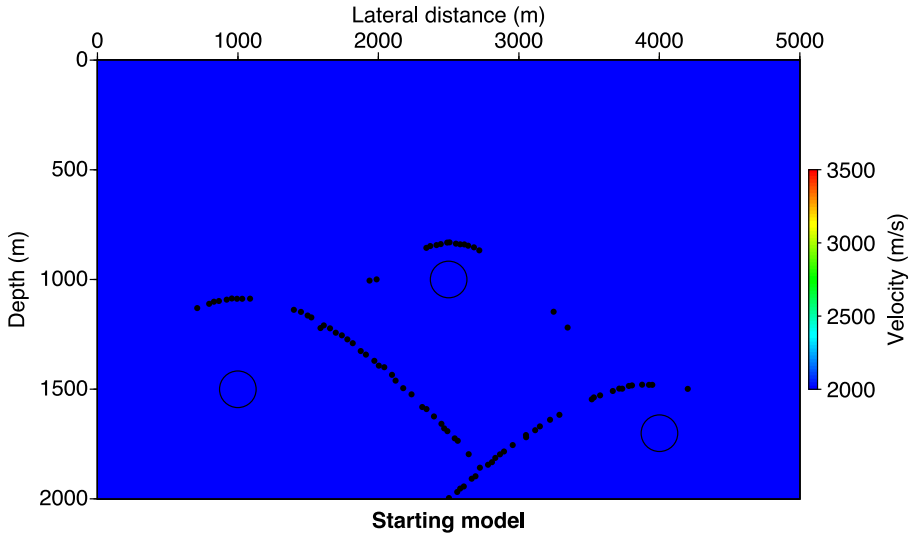

Figure 9: Starting velocity model and the corresponding localization results following from the locally estimated NIP wave attributes t_0, α_0 and R_{NIP}, which are denoted by the black dots. NIP tomography aims at focusing the NIP wave at zero time, which for the active case represents half the zero-offset traveltime. For the considered passive case, the event is supposed to focus at the respective a priori unknown excitation time. The true passive source locations are denoted by the three circles.

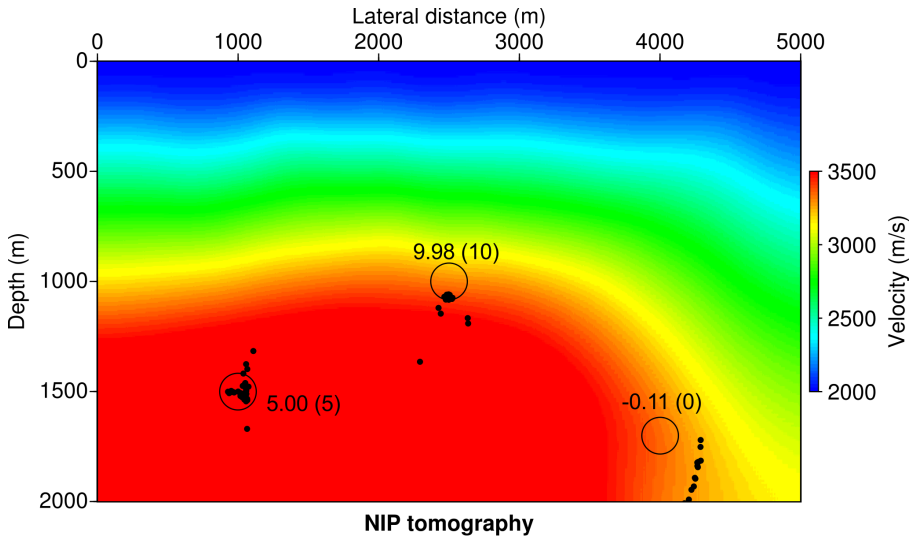

Figure 10: NIP tomographic inversion after 12 iterations. Again, like in Figure 9, the circles denote the true locations of the passive seismic sources. The respective estimated excitation times (shown in seconds) are in reasonable agreement with the exact solution (in brackets). The suggested data-driven strategy based on the CRS attributes not only leads to a reasonable localization, it also jointly provides an estimate of the velocity model in depth. Comparison with the true model shown in Figure 5 reveals that the presented scheme is capable to successfully resolve the general velocity structure traversed by the measured passive seismic events.

CONCLUSIONS AND OUTLOOK

We have presented a fully data-driven stacking scheme for passive seismic event localization in depth, which makes direct use of the formal equivalence of the NIP wave experiment and the actual excitation of a real passive seismic source. Based on a higher-order duality of CRS-type moevoeut approximations, we introduced the 2D passive seismic analog of a generalized diffraction hyperbola, whose application allows for the local estimation of wavefront tilt, curvature and the excitation time of a passive seismic event. By correcting for the estimated source time, the resulting kinematic attributes can directly be fed into the NIP tomographic scheme, which was successfully applied in the context of controlled source data acquisitions with a high data redundancy. To demonstrate the feasibility of the suggested approach, we applied this generalized passive stacking operator to a simple synthetic dataset simulating the sequential recording of three passive seismic events, whose excitation times were assumed to be unknown. The time-shifted version of the passive moveout was shown to be independent of the central ray traveltime, which likewise makes it applicable to active and passive seismic data, the velocity-shifted counterpart allows for a moveout-based inversion of the unknown source time. In the presented data example, the joint application of both moveout formulations led to reasonable estimates of the kinematic wavefield attributes for all three considered events. Starting from a generic constant background, the subsequent application of NIP tomography converged quickly and not only led to a robust event depth localization but it was also able to reasonably recover the heterogeneous velocity structure of the overburden.

A robust estimation of the source excitation time proved to be crucial for a successful localization in depth. Since the presented methodology utilizes a moveout duality, which only shows in orders higher than two, the respective search apertures must be chosen reasonably large, which for complex heterogeneous models may degrade the local character, and therefore, the resolving power of the presented data-driven localization and inversion strategy. Besides the obvious need for an extension to three dimensions, a refinement of the source time estimation will be key to ensure the subsequent applicability of NIP tomography. The current implementation (Duveneck, 2004) allows for a locally independent localization, which in active seismic applications is a reasonable assumption, since for reflections, following Huygens principle, a single event is usually described by a collection of neighboring fictitious point source experiments. In the passive scenario, however, very much like for the diffraction case, an individual event can be related to a single point source (or focus) in depth. The knowledge of the source excitation time is an attribute that globally characterizes a passive event and, therefore, can be used to substantially constrain the NIP tomographic scheme, provided the assumption of a point source is reasonably justified. In addition, the utilized formal correspondence of the active seismic NIP wave concept and the passive seismic ray geometry suggests combined active and passive seismic applications, based on the same simple theoretical framework.

ACKNOWLEDGMENTS

This work was kindly supported by the sponsors of the *Wave Inversion Technology (WIT) Consortium*, Hamburg, Germany, and is part of the project *Imaging steep structures with diffractions* funded by the German Federal Ministry of Economic Affairs and Energy (BMWi 0325363C). Norsar 3D was used to generate the presented data example.

REFERENCES

Baykulov, M. and Gajewski, D. (2009). Prestack seismic data enhancement with partial common-reflection-surface (CRS) stack. *Geophysics*, 74:V49–V58.

Bortfeld, R. (1989). Geometrical ray theory: Rays and traveltimes in seismic systems (second-order approximations of the traveltimes). *Geophysics*, 54(3):342–349.

de Bazelaire, E. (1988). Normal moveout revisited – inhomogeneous media and curved interfaces. *Geophysics*, 53:143–157.

Dell, S. and Gajewski, D. (2011). Common-reflection-surface-based workflow for diffraction imaging. *Geophysics*, 76(5):S187–S195.

Dümmong, S. and Gajewski, D. (2008). A multiple suppression method via CRS attributes. In *SEG Expanded Abstracts*. Society of Exploration Geophysicists.

Duveneck, E. (2004). Velocity model estimation with data-derived wavefront attributes. *Geophysics*, 69(1):265–274.

Fomel, S. and Kazinnik, R. (2013). Non-hyperbolic common reflection surface. *Geophysical Prospecting*, 61(1):21–27.

Gajewski, D., Anikiev, D., Kashtan, B., Tessmer, E., and Vanelle, C. (2007). Seg technical program expanded abstracts 2007.

Gelchinsky, B., Berkovitch, A., and Keydar, S. (1999). Multifocusing homeomorphic imaging – part 1. Basic concepts and formulae. *Journal of Applied Geophysics*, 42:229–242.

Höcht, G., de Bazelaire, E., Majer, P., and Hubral, P. (1999). Seismics and optics: hyperbolae and curvatures. *Journal of Applied Geophysics*, 42:261–281.

Hubral, P. (1983). Computing true amplitude reflections in a laterally inhomogeneous earth. *Geophysics*, 48:1051–1062.

Hubral, P., Schleicher, J., Tygel, M., and Hanitzsch, C. (1993). Determination of Fresnel zones from traveltime measurements. *Geophysics*, 58(5):703–712.

Jäger, R., Mann, J., Höcht, G., and Hubral, P. (2001). Common-reflection-surface stack: Image and attributes. *Geophysics*, 66:97–109.

Landa, E., Keydar, S., and Moser, T. J. (2010). Multifocusing revisited – inhomogeneous media and curved interfaces. *Geophysical Prospecting*, 58:925–938.

Mayne, W. H. (1962). Common reflection point horizontal data stacking techniques. *Geophysics*, 27:927–938.

Nelder, J. A. and Mead, R. (1965). A simplex method for function minimization. *The computer journal*, 7(4):308–313.

Rutledge, J. T. and Phillips, W. S. (2003). Hydraulic stimulation of natural fractures as revealed by induced microearthquakes, Carthage Cotton Valley gas field, east Texas. *Geophysics*, 68(2):441–452.

Schleicher, J., Tygel, M., and Hubral, P. (1993). Parabolic and hyperbolic paraxial two-point traveltimes in 3D media. *Geophysical Prospecting*, 41(4):495–513.

Schwarz, B., Vanelle, C., and Gajewski, D. (2014a). Auxiliary Media - A Generalized View on Stacking. In *76th EAGE Conference and Exhibition*. European Association of Geoscientists and Engineers.

Schwarz, B., Vanelle, C., and Gajewski, D. (2015). Shifted Hyperbola Revisited - The Two Faces of NMO. In *77th EAGE Conference and Exhibition*. European Association of Geoscientists and Engineers.

Schwarz, B., Vanelle, C., Gajewski, D., and Kashtan, B. (2014b). Curvatures and inhomogeneities: An improved common-reflection-surface approach. *Geophysics*, 79(5):S231–S240.

Shearer, P. M. (1990). Seismic imaging of upper-mantle structure with new evidence for a 520-km discontinuity. *Nature*, 344:121–126.

Sheriff, R. E. and Geldart, L. P. (1995). *Exploration seismology*. Cambridge university press.

Taner, M. T. and Koehler, F. (1969). Velocity spectra - digital computer derivation applications of velocity functions. *Geophysics*, 34(6):859–881.

Zhebel, O., Gajewski, D., and Vanelle, C. (2011). Localization of seismic events in 3D media by diffraction stacking. In *73rd EAGE Conference & Exhibition*. European Association of Geoscientists and Engineers.